APPENDIX

$$\rho_{11}^{0}=(2/eN)(\mu_1+\mu_2+2c\nu_1)^{-1},$$

$$\rho_{33}^{0}=(1/eN)(\mu_3+c\nu_3)^{-1},$$

$$\rho_{23,1}=(1/eN)[(\mu_1+\mu_2)\mu_3-\mu_4^2-2c\nu_1\nu_3]\times(\mu_1+\mu_2+2c\nu_1)^{-1}(\mu_3+c\nu_3)^{-1},$$

$$\rho_{12,3}=(4/eN)(\mu_1\mu_2-c\nu_1^2)(\mu_1+\mu_2+2c\nu_1)^{-2},$$

$$\rho_{11,11}=(1/2eN)[(\mu_1-\mu_2)^2\mu_3+(5\mu_1-\mu_2)\mu_4^2]\times(\mu_1+\mu_2+2c\nu_1)^{-2},$$

$$\rho_{11,22}=(1/2eN)(\mu_1+\mu_2+2c\nu_1)^{-2}\{3\mu_1^2\mu_3+(2\mu_1+3\mu_2)(\mu_2\mu_3-\mu_4^2)+\mu_1\mu_4^2+8c\nu_1^2\nu_3-[(\mu_1+\mu_2)\mu_3-\mu_4^2-2c\nu_1\nu_3]^2(\mu_3+c\nu_3)^{-1}\},$$

$$\rho_{11,33}=(2/eN)(\mu_1+\mu_2+2c\nu_1)^{-2}[\mu_1\mu_2(\mu_1+\mu_2)+2c\nu_1^3-4(\mu_1\mu_2-c\nu_1^2)^2(\mu_1+\mu_2+2c\nu_1)^{-1}],$$

$$\rho_{33,11}=(1/2eN)(\mu_1+\mu_2+2c\nu_1)^{-1}(\mu_3+c\nu_3)^{-2}\times\{2(\mu_1+\mu_2)(\mu_3+c\nu_3)^2c\nu_1+\mu_4^2[(\mu_1-\mu_2)\mu_3-\mu_4^2+4c\nu_1(2\nu_3-\mu_3)]\},$$

$$\rho_{33,33}=(1/eN)\mu_1\mu_4^2(\mu_3+c\nu_3)^{-2},$$

$$\rho_{11,23}=(1/eN)\mu_1\mu_4(\mu_1-\mu_2)(\mu_1+\mu_2+2c\nu_1)^{-2},$$

$$\rho_{23,11}=(1/2eN)[(\mu_1-\mu_2)\mu_3\mu_4+\mu_4^3]\times(\mu_1+\mu_2+2c\nu_1)^{-1}(\mu_3+c\nu_3)^{-1},$$

$$\rho_{23,23}=-(1/eN)(\mu_1+\mu_2+2c\nu_1)^{-2}(\mu_3+c\nu_1)^{-1}\times\{\mu_1\mu_2\mu_4^2+2\mu_1\mu_2c\nu_1(\mu_3+c\nu_3)+c\nu_1^2[(\mu_1+\mu_2)\mu_3-\mu_4^2-2c\nu_1\nu_3]\}. \quad \text{(A1)}$$

PHYSICAL REVIEW VOLUME 127, NUMBER 5 SEPTEMBER 1, 1962

Shubnikov-de Haas Effect in Bismuth*†

LAWRENCE S. LERNER‡
Department of Physics and Institute for the Study of Metals, University of Chicago, Chicago, Illinois
(Received April 4, 1962)

The oscillatory component of the transverse magnetoresistance of bismuth has been measured as a function of magnetic field orientation at liquid helium temperatures. A derivative technique was employed. In addition to sets of periods, observed in the de Haas-van Alphen effect by Shoenberg and by Brandt and attributed by them, respectively, to the electron and light-hole Fermi surfaces, we observe a new set of isotropic short periods, $P=0.72\times10^{-5}$ G^{-1}. The squares of the electron Fermi momenta $m_0\kappa_{11}^2$, $m_0\kappa_{22}^2$, $m_0\kappa_{33}^2$, $m_0\kappa_{23}^2$ are, respectively, 0.189, 45.4, 0.918, and -4.54 m_0 milli-electron volts (meV). For the light holes, $m_0\kappa_{11}^2$ and $m_0\kappa_{33}^2$ are 1.51 and 21.0 m_0 meV. For the new heavy carriers, $m_0\kappa^2=3.18$ m_0 meV. These data are fitted to two possible three-carrier models of the Fermi surface, and to a four-carrier model. Significant deviations of the oscillations from periodicity in H^{-1} are observed for the electron part of the Fermi surface for certain magnetic field orientations.

I. INTRODUCTION

THE Fermi surface of the semimetal bismuth has been extensively investigated by means of the de Haas-van Alphen effect[1–6] and other measurements based upon the same quantization condition,[7–16] by means of cyclotron resonance[17–22] and surface resistance measurements,[23,24] and by means of the galvanomagnetic effects.[25–31] In general, the experimental results

* Submitted as a thesis in partial fulfillment of the requirements for the degree of Doctor of Philosophy at the University of Chicago.

† This work was supported in part by a grant from the National Science Foundation.

‡ Now at Hughes Research Laboratories, Malibu, California.

[1] D. Shoenberg and M. Z. Uddin, Proc. Roy. Soc. (London) **A156**, 687 (1936).
[2] D. Shoenberg, Proc. Roy. Soc. (London) **A170**, 341 (1939).
[3] J. S. Dhillon and D. Shoenberg, Phil. Trans. Roy. Soc. London **A248**, 1 (1955).
[4] D. Weiner, Phys. Rev. **125**, 1226 (1962).
[5] N. B. Brandt, A. E. Dubrovskaia, and G. A. Kytin, Soviet Phys.—JETP **10**, 405 (1960).
[6] N. B. Brandt, Soviet Phys.—JETP **11**, 975 (1960).
[7] W. C. Overton and T. G. Berlincourt, Phys. Rev. **99**, 1165 (1955).
[8] J. Babiskin, Phys. Rev. **107**, 981 (1957).
[9] J. M. Reynolds, H. W. Hemstreet, T. E. Leinhardt, and D. D. Triantos, Phys. Rev. **96**, 1203 (1954).
[10] P. B. Alers and R. T. Webber, Phys. Rev. **91**, 1060 (1953).
[11] R. A. Connell and J. A. Marcus, Phys. Rev. **107**, 940 (1957).
[12] D. H. Reneker, Phys. Rev. **115**, 303 (1959).
[13] W. S. Boyle, F. S. L. Hsu, and J. E. Kunzler, Phys. Rev. Letters **4**, 278 (1960).
[14] W. S. Boyle and K. F. Rodgers, Phys. Rev. Letters **2**, 338 (1959).
[15] M. C. Steele and J. Babiskin, Phys. Rev. **98**, 359 (1955).
[16] Y. Eckstein and J. Ketterson (private communication).
[17] J. E. Aubrey and R. G. Chambers, J. Phys. Chem. Solids **3**, 128 (1957).
[18] J. E. Aubrey, thesis, Cambridge University, 1958 (unpublished).
[19] J. K. Galt, W. A. Yager, F. R. Merritt, B. B. Cetlin, and H. W. Dail, Phys. Rev. **100**, 748 (1955).
[20] J. K. Galt, W. A. Yager, F. R. Merritt, B. B. Cetlin, and A. D. Brailsford, Phys. Rev. **114**, 1396 (1959).
[21] R. N. Dexter and B. Lax, Phys. Rev. **100**, 1216 (1955).
[22] Y. H. Kao, J. I. Budnick, and S. H. Koenig, Bull. Am. Phys. Soc. **6**, 439 (1961).
[23] G. E. Smith, Phys. Rev. **115**, 1561 (1959).
[24] G. E. Everett (to be published).
[25] B. Abeles and S. Meiboom, Phys. Rev. **101**, 544 (1956).
[26] A. L. Jain, Phys. Rev. **114**, 1518 (1959).
[27] R. N. Zitter, preceding paper [Phys. Rev. **127**, 1471 (1962)].

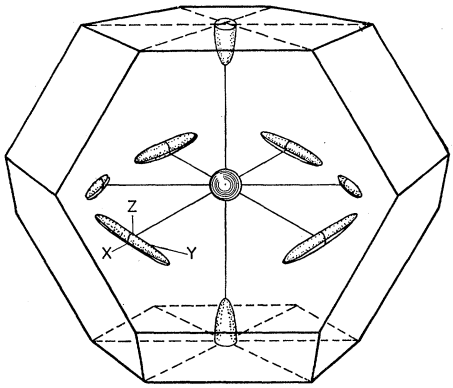

FIG. 1. One possible three-carrier model of the complete Fermi surface in bismuth. The sphere in the center contains heavy holes, the half-ellipsoids of revolution at the trigonal faces light holes, and the six similar ellipsoids electrons.

support a model of the electronic part of the Fermi surface proposed by Jones[32] and elaborated by Shoenberg[2] and by Blount and Cohen.[33] In this model, the electrons lie in several ellipsoidal or quasiellipsoidal[34] surfaces located symmetrically about the trigonal axis in the Brillouin zone (Fig. 1). The long axes of the surfaces make a small angle with the trigonal plane; if they are ellipsoids, they are described by the equation

$$\frac{p_x^2}{m_{11}}+\frac{p_y^2}{m_{22}}+\frac{p_z^2}{m_{33}}+\frac{p_y p_z}{m_{23}}=2m_0\zeta_e \qquad (1)$$

in the coordinate system of the reciprocal lattice, where the subscripts 1, 2, 3 and x, y, z refer, respectively, to the binary, bisectrix, and trigonal axes of the rhombohedral lattice. Experiments are generally in agreement that the electron Fermi energy is $\zeta\approx 20$ milli-electron volts (meV), and that $m_{11}:m_{22}:m_{33}:m_{23}\approx 1:240:5:-24$. The total electron concentration is of the order of 10^{17} cm^{-3}. There is conflicting evidence on the multiplicity of the electron ellipsoids; there are either three or six, and the exact value of the electron concentration is likewise unsettled.

The situation with regard to the hole surfaces is still less satisfactory. Experiments involving the de Haas-van Alphen effect in pure Bi [5,6] and in Bi-Te alloys,[4] the cyclotron resonance,[20] and the galvanomagnetic effects in pure Bi[27] on the one hand, and experiments involving the specific heat[35,36] and the galvanomagnetic effects in Bi-Sb alloys[26,37] on the other hand, give different pictures of the holes. The former group of experiments supports a model of the hole Fermi surface consisting of one or two ellipsoids of revolution lying on the trigonal axis with $m^*\approx 0.16$ and $\zeta\approx 10$ meV. The latter group is more consistent with a picture of the Fermi surface of similar geometry, but with $m^*\approx 1.5$ and $\zeta\approx 1$ meV. This has led to the conjecture that both the light and the heavy holes exist.

Also of interest is the fact that the results of measurements at certain magnetic field orientations in some of the de Haas-van Alphen-type experiments do not fit well into the generally accepted picture of the electron Fermi surface. This is notably true of the measurements of the oscillatory components of the longitudinal magnetoresistance,[8] the transverse magnetoresistance,[7] and the Hall effect.[9]

It is the principal purpose of this paper to present experimental evidence, from the Shubnikov-de Haas effect, that there are at least three and very likely four sets of carriers in bismuth. We have employed a derivative technique to measure dR/dH as a function of H, where R is the electrical resistance of the sample. This method is of especial utility in bismuth, as it removes the extremely large monotonic magnetoresistance upon which the Shubnikov-de Haas oscillations are superimposed.

II. EXPERIMENTAL

Sample Preparation

Bismuth of nominal 99.998% purity[38] was cut into chunks of convenient size, heavily etched in nitric acid, and then washed in a stream of distilled water to remove most of the nitrate on the surface. The bismuth was then placed in a clean fused-silica drip-melting boat, and the boat inserted in the sample tube of a zone refiner. The bismuth was melted in a vacuum of 10^{-5}–10^{-6} torr. The melt was allowed to remain at a temperature of about 400°C for about one-half hour, during which the zone-refiner tube was agitated to assist inclusions of insoluble matter in rising to the surface of the melt. The bismuth was then allowed to drip into a clean, HF-etched fused-silica zone-refining boat through a small hole in the bottom of the drip-melting boat. No scum was observable upon the surface of the drip-melted bismuth, and none accumulated during subsequent operations.

The two boats were then separated, using a vacuum manipulator.[39] After being allowed to freeze, the bismuth was zone refined for 20 passes at a rate of 2 in./h. The boat length was 20 in.; the zone length varied from $\frac{1}{2}$ in. (near the middle of each pass) to

[28] T. Okada, Mem. Fac. Sci. Kyusyu Univ. **B1**, 168 (1955).
[29] T Okada, Mem. Fac. Sci. Kyusyu Univ. **B1**, 157 (1955).
[30] S. Mase and S. Tanuma, J. Phys. Soc. Japan **14**, 1644 (1959).
[31] S. Mase, J. Phys. Soc. Japan **14**, 584 (1959).
[32] H. Jones, Proc. Roy. Soc. (London) **A155**, 653 (1936).
[33] E. I. Blount and M. H Cohen (private communication). For a description of the model, see, e.g., references 26 and 23, or B. Lax, Revs. Modern Phys. **30**, 135 (1958).
[34] M. H. Cohen, Phys. Rev. **121**, 387 (1961).
[35] I. N. Kalinkina and P. G. Strelkov, Soviet Phys.—JETP **7**, 426 (1958).
[36] N. E. Phillips, Phys. Rev. **118**, 644 (1960).
[37] Jain assumes a hole mass $m^*=1.5$ on the basis of the specific heat data of reference 35. However, this value may be obtained directly from Jain's data by means of a more detailed calculation on the Jain model [L. S. Lerner (unpublished)]. The calculation is based on the fact that the hole-electron effective mass ratio determines the height of the hump in Jain's Fig. 8.
[38] Obtained from the Cerro de Pasco Corporation.
[39] D. B. Cowie, Rev. Sci. Instr. **15**, 46 (1944).

TABLE I. Minimum detectable impurity.

ppm	Substances
	(a) By neutron activation analysis
10	Fe, Mg, Ni, Si, Sn
1	Ag, Ba, Cd, Ce, Cr, Mo, Na, Nd, P, Pt, Sr, Te, Tl, W, Zr
0.1	As, Cl, Co, Cs, Cu, Ge, Hg, K, Mn, Os, Ru, Sb, Se, Th, Y, Zn, and all rare earths not specifically mentioned
0.01	Au, Br, Ga, Pd, Rh, Se, Ta, U
0.001	In, Ir, Re, Sm
	(b) By spectrographic analysis
0.1	Fe
0.1	Mg
0.1	Si
10	Ni
20	Sn

about 1 in. (near the ends of each pass). The pressure in the zone refiner was maintained in the range 10^{-6}–10^{-7} torr during the entire process.

The zone-refined ingot appeared upon etching to contain two large crystals. Care was taken during etching and subsequent handling not to subject the ingot to strains.

A sample was cut from near the middle of the ingot and subjected to neutron activation analysis.[40] No impurity was detected down to the limits of sensitivity listed in Table I(a).

A second sample from the middle of the ingot was subjected to spectrographic analysis. No impurity was detected down to the limits of sensitivity. These limits are given in Table I(b) for Si, Fe, Mg, Ni, and Sn, the elements for which the neutron activation method is less sensitive than 1 part per million (ppm). Ni and Sn were not detected spectrographically either in the original material, in the zone-refined ingot, or in the "dirty" ends of the ingot. For these elements, however, the sensitivity of both methods is relatively poor. Reference to the phase diagrams of Bi-Ni and[41] Bi-Sn suggests that the segregation coefficient is appreciably different from unity in both cases, so that Ni and Sn, if present initially, should be removed efficiently by zone refining.

We may conclude from these considerations that the concentration of impurity carriers is small compared with that of intrinsic carriers.

A large single-crystal piece was cut from the ingot and was x-ray oriented to within 1°. Rectangular parallelopipedal samples were cut from it.[42] The final dimensions of the samples are listed in Table II.

[40] The analysis was carried out by a group under the direction of G. W. Leddicotte at the Oak Ridge National Laboratory, to whom the author's thanks are due.

[41] M. Hansen, *Constitution of Binary Alloys* (McGraw-Hill Book Company, Inc., New York, 1958), 2nd ed.

[42] A toothless bandsaw with a 0.004-in. steel blade was used. The cutting agent was a glycerine-water slurry of 600-mesh carborundum powder. The samples were etched in a 50-50 nitric acid-water solution, annealed in silicone oil at 210°C for 24 h, and lightly etched again.

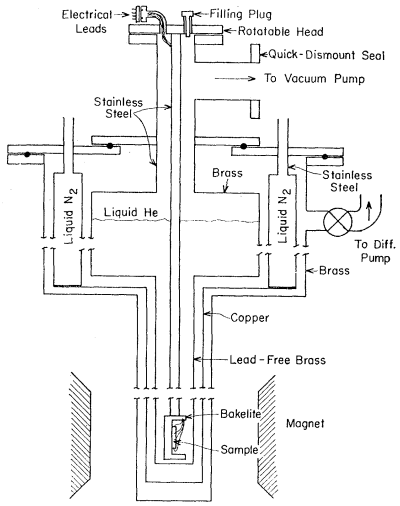

FIG. 2. Cryogenic apparatus and sample holder.

The electrical resistivity ratio $Z \equiv \rho_{300°K}/\rho_{4.2°K}$ was found to be $Z_3 = 120$ and $Z_2 = 200$, respectively, for crystals Bi Ia (current and trigonal axis in long direction) and Bi II (current and bisectrix axis in long direction).[43] These ratios are considerably smaller than those expected for large samples of good purity. The results of Friedman and Koenig,[44] however, indicate that our samples are well into the size-effect region at "zero" magnetic field, so that low resistivity ratios are not necessarily indicative of low purity or excessive cold working. The rather small anisotropy of the ratios is consistent with Friedman and Koenig's observations. It appears from their work that the size effect is only about 25% when the thin direction is a bisectrix, as is the case for our Bi Ia. Friedman and Koenig made measurements only on samples for which the current and the trigonal axis were in the long direction. It is nonetheless to be expected that the size effect be larger in the orientation exemplified by Bi II. In large crystals, Z_2/Z_3 is much larger than 200/120.[27]

TABLE II. Sample dimensions.

Sample	x (mm)	y (mm)	z (mm)
Bi Ia	2.17	1.42	12
Bi Ib	2.17	1.86	12
Bi II	1.97	23	1.46

[43] We would like to remark on the danger inherent in the widespread practice of using resistivity ratios as a criterion of purity in bismuth, due to the very large low-temperature magnetoresistance. We were able to reduce $\rho_{4.2°K}$ for sample Bi Ib by a factor of two merely by surrounding the Dewar with a sheet of $\frac{1}{16}$-in. mu metal. The ambient magnetic field was less than 1 G. For $H \gtrsim 200$ G, the magnetoresistance of Bi Ia at 1.2°K, with $H \| 2$, is $\rho = 13H$ $\mu\Omega$-cm/G. For comparison, the "zero-field" resistivity of Bi Ia is 2 $\mu\Omega$-cm. These crude observations are amply corroborated by the work of Zitter (reference 27).

[44] A. N. Friedman and S. H. Koenig, IBM J. Research Develop. 4, 158 (1960).

Cryostat System and Magnet

Figure 2 is a schematic diagram of the cryostat used in the experiment. The sample is mounted on the bakelite holder with rubber cement in such a way that it is coaxial with the center of rotation of the cryostat cover and lies at the center of the magnetic field. Current and potential leads are soldered onto the sample with Cerroseal 35 low-melting-point solder. The distance between the potential leads is approximately one-third the sample length.

The magnet is a 12-in. Varian electromagnet with pole pieces tapered to 5 in. and a pole gap of $2\frac{1}{8}$ in. The range of magnetic field is 70–15400 G. Two pairs of modulation coils are mounted on the pole pieces, one for small modulation fields and the other for large ones.

Detection System

Figure 3 is a block diagram of the electronic apparatus. The variable resistor is large enough so that the current flow through the bismuth sample, set at 20–100 mA, is nearly independent of the resistance of the sample. The dc magnetic field H is varied smoothly within the range of the magnet.

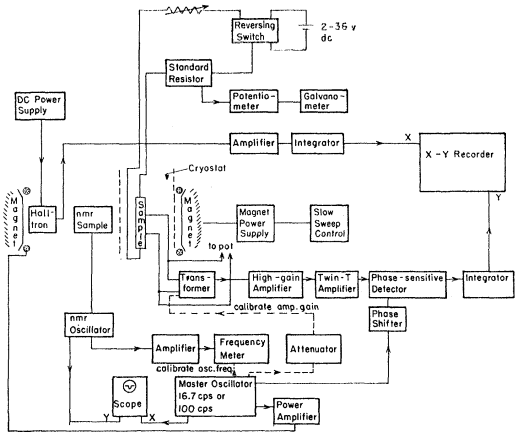

FIG. 3 Block diagram of the electronic apparatus.

An ac signal at 16.7 or 100 cps, applied to the modulation coils, superimposes a small ripple ΔH (=1–5 G) upon the field H. An ac signal is thus induced at the transformer secondary which is proportional to $[\Delta\rho/\Delta H]_H$, where ρ is the resistivity of the sample. The ratio of transformer input impedance to the sample impedance is never less than 10 at maximum H, and is greater for smaller magnetic fields, so that little current is drawn from the sample.

The ac signal is amplified by a narrow-bandpass train of straightforward design, and fed to the Y input of an X-Y recorder.

The X input of the recorder is furnished by a Hall magnetometer, the sensitive element of which is an InAs Halltron.[45] The Hall magnetometer is calibrated and checked periodically during the course of each experimental run by means of a proton-Li^7 nuclear resonance magnetometer, and is linear within 0.1% in the field range of interest.

The output of the Hall magnetometer is fed to the recorder through an integrator, whose purpose is to introduce into the X-input channel a delay time equal to the delay time in the Y-input channel. This makes it possible to sweep the magnetic field rapidly without introducing delay-time errors. Experimental checks at various sweep rates showed that at the fastest sweep rate used, no such errors were observable.

TABLE III. Summary of data.

X-Y plane ψ (deg)	Class of data	Magnetic field range[a]
90 (binary)	IV	LH
$87\frac{1}{2}$	IV	L
85	IV	LH
$82\frac{1}{2}$	IV	L
80	III	LH
75	III	LH
70	III	LH
65	II	LH
$62\frac{1}{2}$	II	L
60 (bisectrix)	II	LH
$57\frac{1}{2}$	II	L
55	III	LH
50	II	LH
45	II	LH
40	III	LH
35	IV	LH
$32\frac{1}{2}$	IV	L
30 (binary)	IV	LH
θ (deg)		
90 (binary)	IV	LH
85	IV	H
80	IV	LH
75	II or IV	H
70	II	LH
65	II	LH
60	II	LH
55	II	LH
50	II	LH
45	III	LH
40	III	LH
35	II	LH
30	III	LH
25	III	L
20	I	L
15	I	LH
10	I	L
5	I	H
0 (trigonal)	I	LH

[a] L: 70–4500 G; H: 70–15400 G.

Experimental Details

Preliminary runs at a few orientations were made in Bi Ia and Bi Ib in order to check reproducibility of data from sample to sample. The latter sample exhibited Shubnikov-de Haas oscillations of slightly greater amplitude. This may have been due to a small drift in the gain of the amplifier or to a difference in the state of internal strain between the two samples.

[45] Model HR-31, manufactured by Ohio Semiconductors Corporation.

However, there was no observable difference in the periods. Further measurements were all made upon Bi Ib and Bi II. These samples were cycled several times each between room temperature and 1.2°K. Aside from a small decrease in oscillation amplitude from the first run to the second the data were completely reproducible from run to run.

Observations made at several magnetic field orientations distributed all around the X-Y plane (Bi Ib) and the X-Z plane (Bi II) were in accordance with the expected trigonal symmetry in the former and binary symmetry in the latter. The detailed analysis was, therefore, restricted to magnetic field orientations in one sextant of the X-Y plane, and in one quadrant of the X-Z plane.

Observations were made at 4.2 and 1.22°K. As expected, the amplitude of the oscillations was considerably greater at the lower temperature, and, as we shall see, certain sets of oscillations visible at the lower temperature were completely absent at the higher. The absolute noise level was somewhat lower at 1.22°K, presumably due to the absence below the λ point of agitation of the sample due to bubbling in the liquid helium.

No differences pertinent to the analysis of the Shubnikov-de Haas effect were apparent upon changing the magnetic field modulation frequency from 16.7 to 100 cps.[46] As the absolute noise level was slightly lower at 16.7 cps, most measurements were made at this frequency.

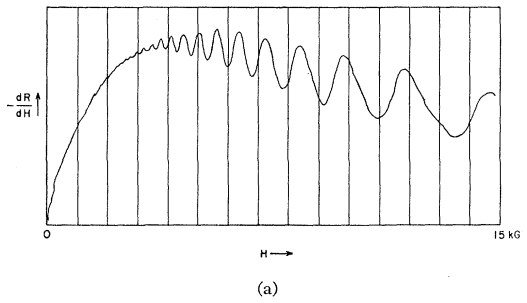

(a)

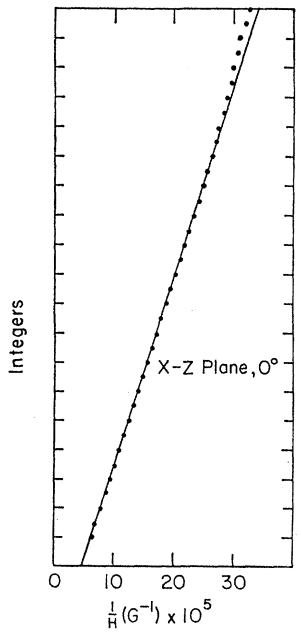

(b)

FIG. 4. (a) Differential Shubnikov-de Haas oscillations for $\theta=0°$. This and the following four figures are freehand tracings of the original data. The smallest-scale irregularities are tracing errors which do not appear in the originals. (b) Plot of reciprocal field values of the maxima and minima of Fig. 4(a) against successive half-integers.

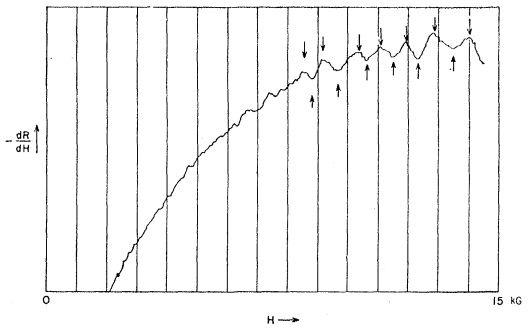

(a)

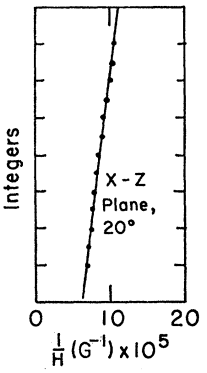

(b)

FIG. 5. (a) Differential Shubnikov-de Haas oscillations for $\theta=20°$. (b) Plot of reciprocal field values of the maxima and minima of Fig. 5(a) against successive half-integers.

III. RESULTS AND ANALYSIS

Experimental runs were made at the magnetic field orientations shown in the first column of Table III. Two types of sweep were employed; one over the entire magnetic field range at a rate of about 35 G/sec, and the other over the range 70–4500 G at a rate of about 10 G/sec, using an expanded magnetometer scale. This latter procedure makes possible more accurate measurements of the low-field oscillations. The type of sweep employed at each orientation is given in the third column of Table III. Four full-range runs are shown in Figs. 4(a), 5(a), 6(a), and 7(a). The first two are

[46] Large single peaks about 35 G wide have been observed at 100 cps, of amplitude comparable to or larger than the oscillations, and superimposed upon them. These peaks appear to persist to higher temperatures than the oscillations, and are invariant under reversal of both H and the current I. Up to three peaks have been observed between 0–15 kG, depending upon orientation. The field H^* at which a peak is seen is I dependent; each peak obeys the empirical relation $H^*=h_0+cI^{-1}$, where h_0 is the same constant for all peaks seen at a given field orientation, and c is a constant for each peak. This phenomenon has also been observed in zone-leveled Bi-Sn alloys containing up to 0.1 wt% Sn.

typical of runs in magnetic field directions where only one period is apparent, and beating effects are absent or negligible. Fig. 5(a) depicts the smallest signal-to-noise ratio encountered in the experiment. The oscillation amplitude is very small because, as we shall see below, these oscillations arise from a group of heavy carriers. Fig. 6(a) is typical of field orientations where beating occurs, but a reliable sorting-out of periods is possible in the later analysis. Fig. 7(a) is typical of field orientations in which beating produces effects so complicated that the meaningfulness of at least some of the individual periods extracted in the analysis is open to considerable doubt. These three sorts of data are called class I, class II, and class III, respectively. A fourth class of orientations, class IV, is typified by Fig. 8(a). The class IV oscillations possess the general characteristics of either class I or II, but also have properties associated with the peculiar line shape evident upon inspection of Fig. 8(a). We will discuss the class IV oscillations in detail later. The assignment of the various field orientations into the above four classes is given in the second column of Table III.

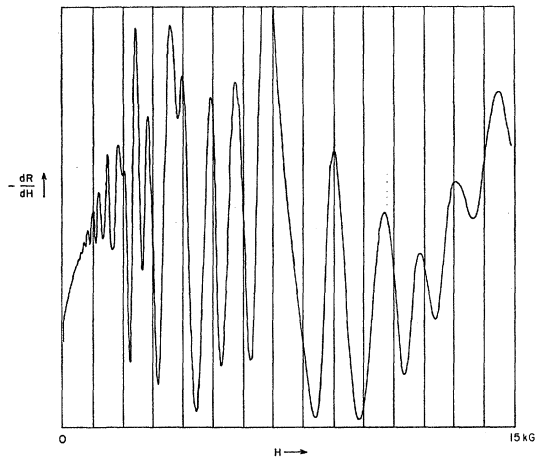

(a)

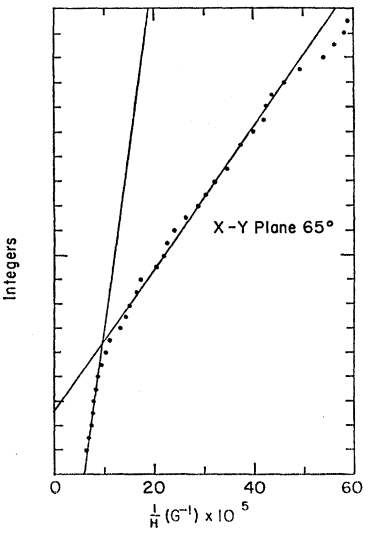

(b)

FIG. 6. (a) Differential Shubnikov-de Haas oscillations for $\psi=65°$. (b) Plot of reciprocal field values of the maxima and minima of Fig. 6(a) against successive half-integers.

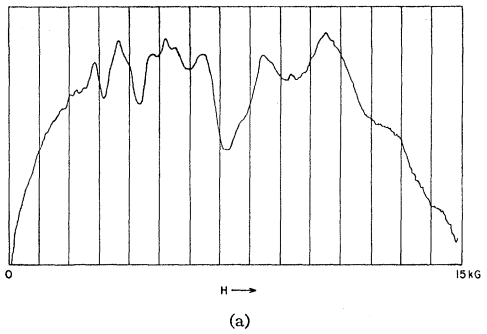

(a)

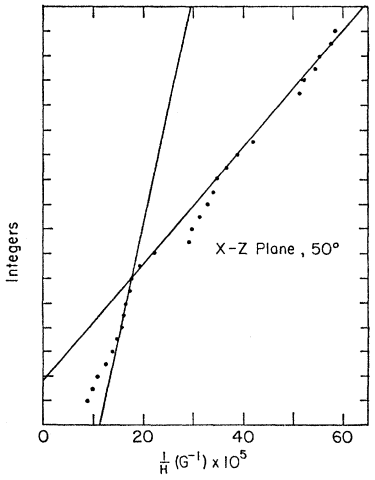

(b)

FIG. 7. (a) Differential Shubnikov-de Haas oscillations for $\theta=50°$. (b) Plot of reciprocal field values of the maxima and minima of Fig. 7(a) against successive half-integers.

For each magnetic field orientation, the H values and the corresponding H^{-1} values of the oscillation maxima and minima were computed from the Hall magnetometer calibration curve. These H^{-1} values were then plotted against successive half-integers, as in Figs. 4(b), 5(b), 6(b), 7(b), and 8(b). The oscillations periodic in various values of H^{-1} were separated, when possible, by observing the breaks in the lines. The slopes $\Delta(H^{-1})$ of the straight segments are plotted as a function of magnetic field orientation in Fig. 9. For comparison, Shoenberg's data[2] are shown as crosses. That his values lie slightly above ours is presumably due to a difference in impurity content. As was mentioned above, in the class III directions the ratio of the periods of two or more oscillatory components of similar amplitude is such that very complicated beating results. The computed periods may, therefore, be greatly in error or spurious. This is usually true only over part of the magnetic field range. Such doubtful periods are plotted as dashed points in Fig. 9. In the case of certain orientations [e.g., that of Fig. 6(a)], long periods can

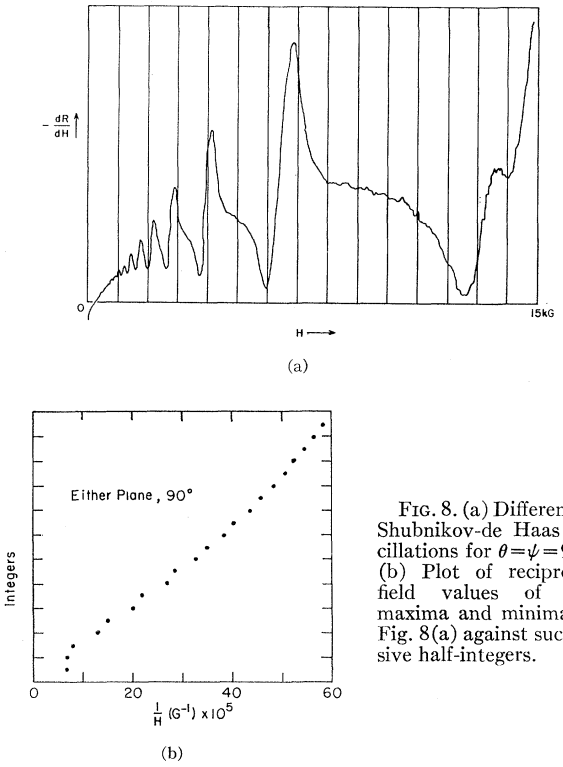

FIG. 8. (a) Differential Shubnikov-de Haas oscillations for $\theta=\psi=90°$. (b) Plot of reciprocal field values of the maxima and minima of Fig. 8(a) against successive half-integers.

be extracted from the beats. This is an especially reliable procedure where the long periods are close to integral multiples of the shorter ones. The long periods for $\psi=50°$, $57\frac{1}{2}°$, $60°$, $62\frac{1}{2}°$, and $65°$ are of this sort.

IV. DISCUSSION

General Remarks

The period $\Delta(H^{-1})$ of the de Haas-van Alphen oscillations is equal to eh/cA, where A is the extremal cross-sectional area normal to the magnetic field of a piece of Fermi surface in **k** space.[47] For an ellipsoidal Fermi surface,

$$A_{ij}=\pi m_0\kappa_i\kappa_j \tag{2}$$

in the principal axis system. Here κ_i and κ_j are proportional to the carrier Fermi momenta in the mutually perpendicular i and j directions normal to H_k, and

$$\kappa_{i,j}{}^2=2m_{i,j}{}^*\zeta. \tag{3}$$

The symbols m_0, $m_{i,j}$, and ζ stand, respectively, for the free electron mass, the carrier effective mass ratio in the i or j direction, and the Fermi energy, measured from the band edge and taken positive, as usual. If there are several pieces of Fermi surface, as is the case in bismuth, the observed oscillations will usually be a composite of the individual components.

[47] A. H. Kahn and H. P. R. Frederikse, in *Solid State Physics* edited by F. Seitz and D. Turnbull (Academic Press Inc., New York, 1959), Vol. 9, p. 257.

The theory of the de Haas-van Alphen-like oscillations in other properties (including transverse magnetoresistance) has not achieved the same state of sophistication as that for the susceptibility oscillations. However, there is ample experimental[15,47] and theoretical[47] evidence that these oscillations also are periodic in $\Delta(H_k^{-1})=eh/cA_{ij}$. We find this to be the case for all our experimental data except for the class IV points.

The Electron Fermi Surface

According to the three- or six-ellipsoid model, the angular dependence of the periods associated with the electron surfaces of bismuth is given in the coordinate system of the reciprocal lattice by the expressions

$H\perp$ trigonal (X-Y plane)

$$P_{\psi_1}=(e\hbar/\nu c)(\kappa_1{}^2\cos^2\psi+\kappa_2{}^2\sin^2\psi)^{\frac{1}{2}}, \tag{4a}$$

and two similar expressions differing in phase from Eq. (4a) by $\pm 60°$, and

$H\perp$ bisectrix (X-Z plane)

$$P_{\theta_1}=(e\hbar/\nu c)(\kappa_3{}^2\cos^2\theta+\kappa_1{}^2\sin^2\theta)^{\frac{1}{2}}, \tag{4b}$$

$$P_{\theta_{2,3}}=\frac{e\hbar}{\nu c}\left(\kappa_3{}^2\cos^2\theta+\frac{\kappa_1{}^2+3\kappa_2{}^2}{4}\sin^2\theta \pm\sqrt{3}\kappa_4{}^2\sin\theta\cos\theta\right)^{\frac{1}{2}}, \tag{4c}$$

where

$$\nu^2=\tfrac{1}{4}m_0\kappa_1{}^2(\kappa_2{}^2\kappa_3{}^2-\kappa_4{}^4). \tag{4d}$$

In the above expressions, ψ is measured from a binary axis, and θ from the trigonal axis. We follow the convention of using κ_1, κ_2, κ_3, and κ_4 as abbreviations for the momentum tensor components κ_{11}, κ_{22}, κ_{33}, κ_{23}, respectively.[48] The parameter κ_4 results from the fact that the electron ellipsoids are slightly tilted out of the X-Y plane.

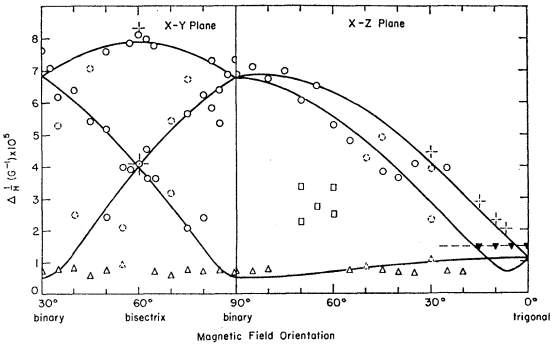

FIG. 9. Shubnikov-de Haas periods as a function of magnetic field orientation. Solid curves are the best fit of the ellipsoid model for the electrons. The dashed line traces part of the light-hole ellipsoid. Circles are electron periods, full triangles light-hole periods, open triangles heavy-carrier periods. Squares are unexplained. Crosses are Shoenberg's data. Dashed points are uncertain.

[48] All other components are zero.

We may now in principle adjust the κ_i in order to obtain the best fit to the circles in Fig. 9. Unfortunately, even to determine the *shape* of the electron surfaces (i.e., the anisotropy of the Fermi momentum) from our data is an inaccurate process. This is because the periods associated with the electron surfaces are inaccurate for the class IV oscillations near the binary axis, since they are not strictly periodic in H^{-1}, and the oscillations observed for H near the trigonal axis are not associated with the electrons. These facts interfere with a determination of κ_1 and κ_3, and since the effect of the "tilt parameter" κ_4 is largest for H near the trigonal axis, it, too, cannot be accurately determined from our data.

Since we are unable to derive the κ_i directly from the data, we proceed as follows. From Eq. (3) we see that the κ_i can be found if we know the m_i and ζ_e. Fortunately, cyclotron resonance experiments furnish us with reliable electron effective mass data. We adopt the values given by Aubrey[18]: $m_1=0.00495$, $m_2=1.19$, $m_3=0.024$, $m_4=-0.119$. These values are in good agreement with those of Kao,[22,49] obtained at higher frequencies. We are still at liberty to adjust the Fermi energy in order to obtain the best fit to our experimental data. If we fix ζ_e at 19.1 meV we obtain the solid curves of Fig. 9, with principal periods $P_x=0.51\times10^{-5}$ G^{-1}, $P_y=7.89\times10^{-5}$ G^{-1}, $P_z=1.12\times10^{-5}$ G^{-1}. With a few exceptions, most of which are class III or class IV points, the experimental circles fit the curves quite well. The points in the X-Z plane tend to fall somewhat below the curves. This may be accounted for by a misalignment of the crystal of 0.2°. Our best values of the κ_i^2 are listed in Table V. The closeness of our periods to the curves at all field orientations is indicative of the agreement of our measurement of the anisotropy of the Fermi surface with Aubrey's.

Our value of ζ_e agrees well with that of Shoenberg and Uddin,[1] who give $\zeta_e=17.7$ meV. We estimate our error to be $\pm5\%$. Shoenberg and Uddin quote an internal error of 2%. If, however, we include the effect of impurities, it is reasonable to assume that their error is also of the order of 5%.

The above argument is based upon the assumption that the electron Fermi surfaces are ellipsoidal in shape, and that the bands are parabolic, i.e., that the m_i are independent of energy near the Fermi level. If this is not the case, ζ_e is not the true Fermi energy. Weiner's experiments in Bi-Te alloys,[4] as well as infrared magnetoreflection experiments,[50,51] indicate that deviation from parabolicity must be taken into account. Consistency of results with theory is achieved by Weiner's employing case A of the Cohen model.[34] Using the same model, we can calculate the value of the true Fermi energy η. We have

$$\eta=\zeta_e+(\epsilon/2)\{[(2\zeta_e/\epsilon)^2+1]^{\frac{1}{2}}-1\}, \qquad (5)$$

where $\epsilon=46$ meV is[4] a parameter related to a small energy gap located near the Fermi level. It is identical to Weiner's E_g/λ. Inserting our value of ζ_e into Eq. (5), we obtain $\eta=26.0$ meV, compared with Weiner's value $\eta=22$ meV.

We now calculate the number of electrons per ellipsoid. For the parabolic-ellipsoidal model,

$$n_e=(8\pi/3h^3)m_0^{\frac{3}{2}}\kappa_1(\kappa_2^2\kappa_3^2-\kappa_4^4)^{\frac{1}{2}}. \qquad (6)$$

Inserting our experimental values, we obtain $n_e=1.01\times10^{17}$ cm^{-3} ellipsoid^{-1}. For the ellipsoidal-nonparabolic model discussed above, the number of electrons per ellipsoid is

$$n_e'=n_e\{1+(1/5)[(\eta/E_g)/(1+\eta/E_g)]\}. \qquad (7)$$

Here E_g is the only energy gap near the bottom of the conduction band comparable in magnitude to the Fermi energy. It is identical to Weiner's E_g.[4] Wolff[52] has estimated that $E_g=42$ meV. Hence, $n_e'=1.09\times10^{17}$ cm^{-3}-ellipsoid^{-1}. This is the value which we shall use in what follows.

The Light-Hole Fermi Surface

According to the theory of the de Haas-van Alphen effect,[53] the amplitude of the oscillations is proportional to $\exp[-\pi km^*c(T+\Delta T)/ehH]$. Here ΔT is an effective temperature related to the collision time. Calculation shows that it is to be expected that no oscillations arising from carriers heavier than the electrons were observed until measurements were made at adiabatic demagnetization temperatures.[5,6]

No such complete theory exists for the oscillations in the transport properties. The quantitative behavior of the amplitude dependence is quite different than that for the susceptibility, and must depend upon the magnetoconductivity tensors $\boldsymbol{\sigma}(\mathbf{H},\mathbf{j})$ associated with the various carriers.

TABLE IV. Oscillation periods in transport experiments, $H\|$trigonal axis.

Experiment	Period (G^{-1})$\times10^5$
Longitudinal magnetoresistance[a]	1.58
Longitudinal magnetoresistance[b]	1.6
Longitudinal magnetoresistance[c]	1.5
Longitudinal magnetoresistance[d]	1.57
Hall effect[e]	1.5
Hall effect[b]	1.6
Present work	1.54±0.02

[a] See reference 8.
[b] See reference 11.
[c] S. Tanuma (private communication).
[d] See reference 7.
[e] See reference 9.

[49] Y. H. Kao (private communication).
[50] R. J. Keyes, S. Zwerdling, S. Foner, H. H. Kolm, and B. Lax, Phys. Rev. **104**, 1804 (1956).
[51] R. N. Brown, J. G. Mavroides, M. S. Dresselhaus, and B. Lax, in *The Fermi Surface*, edited by W. A. Harrison and M. B. Webb (John Wiley & Sons, Inc., New York, 1960), pp. 203–209.
[52] P. Wolff (unpublished).
[53] E. H. Sondheimer and A. H. Wilson, Proc. Roy. Soc. (London) **A210**, 173 (1951).

We now turn to the experimental data. The oscillation periods observed in various transport experiments with H parallel to the trigonal axis are summarized in Table IV. These periods are in close mutual agreement and, moreover, correspond to the de Haas-van Alphen periods observed by Brandt *et al.*[6] and attributed by them to the light holes. Why the light holes should be observed near the trigonal axis to the exclusion of the electrons in the transport effects and not at all in the susceptibility at 1.22°K, we cannot at present explain. We also observe periods of 1.53×10^{-5} G^{-1} at $\theta=5°$, 1.52×10^{-5} G^{-1} at $\theta=10°$, and 1.51×10^{-5} G^{-1} at $\theta=15°$. The experimental uncertainty is only $\pm0.02\times10^{-5}$ G^{-1}. That these periods (the full triangles in Fig. 9) are indeed due to the light holes may be argued as follows:

(a) The data are of class I, and hence the $\Delta(H^{-1})$ are known with high accuracy. The periods are too large to be the electron periods expected on the basis of the Shoenberg model (1.2×10^{-5} G^{-1}).

(b) Three branches of the electron-period curves converge for H parallel to the trigonal axis. They are quite close together over the entire 15° range in which we observe the oscillations in question. If the electron periods were at all observable, all three branches would be seen with about equal amplitudes, and very complicated (class III) beating would be observed. This is not the case. We note, however, that the low-field (high H^{-1}) points in Fig. 4(b) do show more deviation from the straight-line behavior than the points at higher fields. This suggests the possibility that at low fields the electrons make a sufficient contribution to the oscillations to produce beating against the light-hole oscillations and to distort the measured hole periods.

(c) At low magnetic fields,[27] $\Delta\rho\propto H^2$. We observe that at high magnetic fields $\rho\propto H$. We call this the high-field range. At intermediate fields, $\rho\propto H^p$ where $1<p<2$. Whatever the detailed conditions for transition from one range to another may be, they must be of the form $\omega\equiv eH/m^*c=\chi$, where m^* is an appropriate effective mass and χ is some characteristic parameter. If we assume that the transition conditions (i.e., the values of χ) are not very different for the different types of carriers in bismuth, it follows that the transitions will occur at higher magnetic fields for carriers of larger effective masses.

We compare Fig. 4(a), which, we argue, depicts dominant light-hole periods, with Fig. 6(a) (dominant electron periods). Ignoring the oscillations, we note that the high-field range begins in the former at higher magnetic fields ($\approx$4200 G) than in the latter ($\approx$2000 G). This is to be expected in the light of the argument we have just made since, as we will see, the light holes are heavier than the electrons.

We cannot follow these light-hole oscillations beyond 15° from the trigonal axis. Let us assume nevertheless that the light-hole Fermi surface is an ellipsoid of revolution with its axis in the trigonal direction and an areal ratio $A_{12}/A_{23}=3.74$, or an axial ratio $\kappa_3^2/\kappa_1^2=14.0$. These values are calculated from the de Haas-van Alphen results of Brandt *et al.*,[15] who give $m_1=m_2=0.05$, $m_3=0.7$. It is interesting to note that while the effective masses of Galt *et al.*[19] ($m_1=m_2=0.068$, $m_3=0.935$) differ considerably from those of Brandt *et al.*, their ratios $A_{12}/A_{23}=3.72$ and $m_3/m_1=13.8$ are in excellent agreement. Complete agreement of the two sets of effective masses may be obtained by altering Brandt's Fermi energy ζ_h from 16 meV to 11.8 meV. Brandt *et al.* obtain the effective masses, and hence the Fermi energy, from the temperature dependence of the oscillation amplitude. At adiabatic demagnetization temperatures, high accuracy is very difficult to obtain.

Using our value of A_{12} and Brandt's areal ratio, and employing the expression

$$n_h=\frac{8\pi}{3h^3}m_0^{\frac{3}{2}}\kappa_1^2\kappa_3=\frac{8}{3\pi^{\frac{1}{2}}h^3}A_{12}^{\frac{3}{2}}\left(\frac{A_{23}}{A_{12}}\right), \tag{8}$$

we may now calculate the number of light holes per ellipsoid. We obtain $n_h=3.47\times10^{17}$ cm^{-3} ellipsoid^{-1}. The most reliable value of the light-hole Fermi energy ζ_h may be obtained from our κ_1^2 and the cyclotron masses of Galt *et al.*, using the definition of κ. These values yield $\zeta_h=11.1$ meV, in good agreement with the value 11.8 meV obtained above by a comparison of the cyclotron resonance results with the de Haas-van Alphen results of Brandt *et al.*

The Isotropic Fast Oscillations

We now discuss the open triangles of Fig. 9. The period is in each case (except for two of the three dashed points) within 10% of 0.72×10^{-5} G^{-1}. These fast oscillations are either associated with an as yet unobserved feature of the electron or the light-hole Fermi surface, or else are associated with another piece of Fermi surface which is spherical within $\pm10\%$. If the former is the case, the distortion of the electron or light-hole Fermi surface must take the form of a bulge of approximately spherical shape, since the oscillations in question have the smallest period which we observe, and must therefore be associated with a large cross-sectional area A. Brandt[6] observes no such deviation from ellipsoidal form in the light-hole surface. We have been unable to devise a Fermi surface geometry consistent both with Brandt's observations and with our fast oscillations. There is indeed experimental evidence for a deviation of the electron surface from ellipsoidal form,[21] but this deviation takes the form of a slight constriction of the waist of the surfaces (see Fig. 1) rather than a bulge. If there were a bulge, it would result in the absence of the large periods which Shoenberg and we observe in the region of the bisectrix axis (Fig. 9).

We are thus left with the alternative that the fast oscillations are associated with a separate (and spherical) piece of Fermi surface. We argue that this piece of

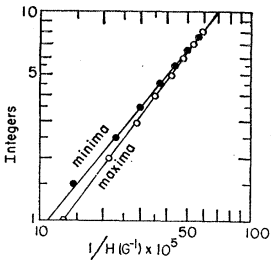

FIG. 10. Log-log plot of Fig. 8(b). The integers are the ordinal numbers of the oscillations starting at small H^{-1}. They have been chosen so as to make the maxima and minima fall on straight-line plots.

Fermi surface contains heavy carriers on the grounds that:

(a) The fast oscillations are not visible at 4.2°K. This rapid disappearance of the oscillations with rising temperature is suggestive of a large effective mass.

(b) The amplitude of the fast oscillations at 1.22°K is two orders of magnitude smaller than that of the oscillations associated with electrons or light holes.

(c) At magnetic field orientations where the fast oscillations dominate (e.g., $\theta=20°$, see Fig. 5) the magnetoresistance enters the high-field range at approximately 12 000 G, a field very much larger than is the case for the orientations where the electrons or light holes dominate.

For a spherical Fermi surface, $A_{ij}=\pi m_0\kappa^2=eh/cP$. Using this expression and the value $P_H=0.72\times10^{-5}$ G^{-1} yields a heavy carrier concentration $n_H=2.88\times10^{17}$ cm^{-3} ellipsoid^{-1}. Here the subscript H refers to the heavy carriers.

The Class IV Points

We now discuss the class IV oscillations in more detail. Reference to Table III shows that they occur within about $12\frac{1}{2}°$ of the binary axis. Figure 8 is typical of class IV. Discounting the small jog at approximately 14 000 G, which may be attributable to spin splitting, we see that the trace possesses two anomalous characteristics. First, the line shape develops a marked asymmetry at high fields. Second, there is a smooth and marked deviation from the periodicity in H^{-1} characteristic of de Haas-van Alphen oscillations. This phenomenon has been noted by Babiskin in the longitudinal magnetoresistance[8] and by Tanuma in the transverse magnetoresistance.[54]

By making trial log-log plots of Fig. 8(b), we can indeed show that the oscillations of Fig. 8(a) constitute a complete set, i.e., that no more oscillations of this group would be observed if we could go to higher fields. Note that the straight line in Fig. 10 is achieved by assigning to the highest field oscillation the ordinal number one. This conclusion is borne out by inspection of Babiskin's Fig. 5, which traces the longitudinal magnetoresistance up to 60 kG. The complete theory of the de Haas-van Alphen effect predicts deviation from the simple periodic behavior for the one or two oscillations nearest the high-field limit, and the previously observed deviations have been qualitatively ascribed to this effect. Our data, however, show that the deviation from simple behavior is observable for at least seven oscillations from the high-field limit, so that it is not possible to explain the deviation on the basis of de Haas-van Alphen theory. The deviation has not been observed in the de Haas-van Alphen effect, but detailed observations have not been made near the binary axis. Also, the peculiar line shape which we observe would tend to be emphasized by a derivative technique. A fairly detailed theory of the Shubnikov-de Haas effect will probably be necessary for an understanding of the class IV data. We can see from Fig. 10 that the maxima are periodic in $H^{-1.2}$ and the minima in $H^{-1.4}$ for H along the binary axis. The exponent appears to approach -1 as the angle between the field and the binary axis increases; unfortunately, the presence of beats for off-binary orientations makes a more precise statement impossible.

The five points in Fig. 9 marked as squares do not fit into any model of the Fermi surface so far proposed, nor do they offer sufficient basis for postulating another piece of Fermi surface. Nevertheless, we have not been able to show that they are spurious periods produced by beating effects. We offer no explanation for them.

The Complete Fermi Surface

We have now determined n for each of the three types of carriers. By requiring over-all electrical neutrality and assuming that there are no other types of carriers, we may deduce the multiplicities q of the three partial Fermi surfaces. On the basis of this procedure, we will deduce two possible three-carrier models.

The existence of the third set of carriers makes it possible to account for the large values reported for the carrier specific heat γ.[35,36] The light-electron-and-light-hole models heretofore proposed fail to do so.

From a value of γ, we may deduce the heavy carrier effective mass and Fermi energy for each of the two three-carrier models. As the two published values of γ are at variance, we shall be obliged to discuss them at some length.

On the basis of his very accurate galvanomagnetic measurements, Zitter[27] has proposed a model of the Fermi surface which is irreconcilable with either of our three-carrier models. We shall show how Zitter's results and ours may be brought into agreement on the basis of a four-carrier model, and we shall deduce some characteristics of that model.

The Three-Carrier Model

If there are only three types of carriers, we may write the electrical neutrality condition

$$q_e n_e' = q_h n_h + q_H n_H, \tag{9}$$

[54] S. Tanuma (private communication).

TABLE V. Summary of results.

	Electrons	Light holes	Heavy carriers
κ_1^2 (meV)	0.189	1.51	3.18
κ_2^2 (meV)	45.4	1.51	3.18
κ_3^2 (meV)	0.918	21.0	3.18
κ_4^2 (meV)	−4.54	0	0
n' or n (cm^{-3}-ellipsoid^{-1})[a]	1.09×10^{17}	3.47×10^{17}	2.88×10^{17}
η or ζ (meV)[a]	26.0	11.1	see below
m_1	4.95×10^{-3} [b]	0.068[c]	see below
m_2	1.19[b]	0.068[c]	
m_3	0.024[b]	0.935[c]	
m_4	−0.119	0	

	Electrons	Light holes	Heavy holes
q	6	1	1
N' or N (cm^{-3})[a]	6.54×10^{17}	3.47×10^{17}	2.88×10^{17}
γ (eV-deg^{-2}-cm^{-3})	0.918×10^{12}	1.14×10^{12}	16.4×10^{12} [d] 4.09×10^{12} [e]
η or ζ (meV)[a]	26.0	11.1	0.63[d] 2.42[e]
m^*	see above	see above	2.5[d] 0.66[e]

	Electrons	Light holes	Heavy electrons
q	3	2	−1
N' or N (cm^{-3})[a]	3.27×10^{17}	6.94×10^{17}	2.88×10^{17}
γ (eV-deg^{-2}-cm^{-3})	0.459×10^{12}	2.28×10^{12}	15.8×10^{12} [d] 3.41×10^{12} [e]
η or ζ (meV)[a]	26.0	11.1	0.60[d] 2.00[e]
m^*	see above	see above	2.6[d] 0.80[e]

	Electrons	Light holes	Heavy carriers 1	Heavy carriers 2
$\lvert q\rvert$	3	1	$\geq\lvert\pm2\rvert$	$\geq\lvert\mp1\rvert$
N' or N (cm^{-3})[a]	3.27×10^{17}	3.47×10^{17}	$2.88\times10^{17}\times q_1 \equiv N_1$	N_1
γ (eV-deg^{-2}-cm^{-3})	0.459×10^{12}	1.14×10^{12}	16.9×10^{12} [d] 4.55×10^{12} [e]	
η or ζ (meV)[a]	26.0	11.1	>1.20[d,f] >4.00[e,g]	>0.60[d,f] >2.00[e,g]
m^*	see above	see above	<1.3[d] <0.4[e]	<2.6[d] <0.8[e]

[a] n', N', and η refer to the light electrons, n, N, and ζ to all other carriers.
[b] See reference 18.
[c] See reference 19.
[d] $\gamma=18.5\times10^{12}$ eV deg^{-2} cm^{-3}.
[e] $\gamma=6.15\times10^{12}$ eV deg^{-2} cm^{-3}.
[f] $q_1(\zeta_1^{-1}+\zeta_2^{-1})=1.67$ meV^{-1}.
[g] $q_1(\zeta_1^{-1}+\zeta_2^{-1})=0.49$ meV^{-1}.

where $N_i\equiv q_i n_i$ and $N_e'\equiv q_e n_e'$ are the total concentrations of the various carriers. Now q_e and q_h must be strictly positive integers; q_H must be a nonzero integer, and will be positive or negative depending upon whether the heavy carriers are holes or electrons. Symmetry properties impose the condition that q_e be divisible by 3. Inserting our numerical results for n_e', n_h, and n_H, we find that Eq. (9) is satisfied within 3% by the multiplicities $q_e=6$, $q_h=1$, and $q_H=+1$. If we use N_e instead of N_e' in Eq. (9), the agreement is to within 5%. The experimental error is ±12%; we cannot, therefore, distinguish between the parabolic and nonparabolic models on the basis of this experiment for the $q_e=6$ model. The multiplicities $q_e=3$, $q_h=2$, $q_H=-1$ satisfy Eq. (9) within 13% if we use n_e'; n_e fails to satisfy electrical neutrality within experimental error in this case.

Comparing the two models, it appears somewhat more likely that the heavy carriers are holes. The N_i are given in Table V for both models. The six-electron-ellipsoid model is illustrated in Fig. 1. The electron ellipsoids are disposed in the Brillouin zone in the manner proposed by Smith.[23,55] Because q_h and q_H are unity, symmetry requirements limit the location of the light-hole ellipsoid and the heavy-hole sphere to either the center of the zone or to the regions of intersection of the trigonal axis with the zone faces. The light-hole and heavy-hole surfaces may not be superimposed; there are no overlapping bands in bismuth.[56] We are

[55] Note that this disposition is one of two possible. The other possibility consistent with symmetry conditions is to locate the electron ellipsoids at the reflection planes, i.e., the points σ in Fig. 1 of reference 34.
[56] M. H. Cohen (private communication).

thus left with two possible permutations of the hole surfaces; in Fig. 1 we have arbitrarily depicted the heavy holes at the zone center and the light holes at the zone faces.

If there are three light-electron ellipsoids ($q_e=3$), the heavy carriers are electrons, and may again lie either at the zone center or at the trigonal faces. The two light-hole ellipsoids may then lie at two symmetrical points on the trigonal axis.

The experimental results yield directly a value for κ for the heavy carriers. In the absence of other undetected carriers, we may use the specific heat to calculate their Fermi energy ζ_H and their effective mass m^*. The coefficient of the term in the expression for the specific heat of a metal which is linear in T is due to the carriers, and is, for three carriers,

$$\gamma=\tfrac{1}{2}\pi^2k^2\left[\frac{N_e'}{\eta}+\frac{N_h}{\zeta_h}+\frac{N_H}{\zeta_H}\right], \tag{10}$$

where k is Boltzmann's constant. The value of γ has been determined experimentally by Kalinkina and Strelkov[35] to be 19.6×10^{12} eV deg^{-2} cm^{-3} and by Phillips[36] to be 6.15×10^{12} eV deg^{-2} cm^{-3}. The latter's results indicate a nuclear quadrupolar contribution to the total specific heat which could not be separated from γ by the former because of the higher temperature range of their experiment ($T\geqslant0.3$°K, compared with Phillips's $T\geqslant0.1$°K). Using Phillips's value for the nuclear quadrupole contribution, we have recalculated Kalinkina and Strelkov's value of γ; we obtain $\gamma=18.5\times10^{12}$ eV deg^{-2} cm^{-3}.

The value of γ is critically dependent upon the quantity and nature of the impurities in the bismuth sample. Owing to the very low intrinsic carrier concentration, a donor or acceptor concentration of approximately 30 ppm in one of the samples would suffice to account for the difference between the two experimental results, after the quadrupole contribution has been accounted for. Phillips gives the impurity content of his sample as a nominal 10 ppm; it is, unfortunately, not clear whether the major impurities would act as donors or acceptors in bismuth.

Kalinkina and Strelkov base their results upon a sample prepared by several recrystallizations from spectroscopically pure bismuth. They report a residual resistivity ratio $\rho_{300°K}/\rho_{4.2°K}$ of 210, which is consistent[57] with a purity similar to that of our samples and considerably greater than that of Phillips's sample. We will nevertheless carry out the subsequent calculations for both values of γ. Using these γ's, η, ζ_h, and the N_i appropriate to each of the two three-carrier models proposed, we obtain the values of ζ_H given in Table V. These, with our value of κ_H^2, yield the values of m_H given in Table V.

In any case the light electrons and light holes alone do not account for the specific heat. If we assume the larger value of γ to be correct and q_H to be zero, no reasonable values of q_e and q_h will satisfy Eq. (10). If we assume the smaller value of γ and $q_H=0$, even $q_e=6$ and $q_h=2$ cannot account for the specific heat.

[57] Subject to the reservations noted above.

The Four-Carrier Model

We have observed three groups of oscillations, which we have ascribed to three kinds of Fermi surface, containing electrons, light holes, and heavy carriers. Upon the assumption that there are no other carriers, two sets of choices of the multiplicities q have been shown to be consistent with the electrical neutrality condition. Aside from our data and the specific heat results, the existence of heavy carriers is supported by the high-field magnetoresistance work of Tanuma[54] and the transport measurements of Sybert *et al.*[58]

There is nothing in any of this work, however, which precludes the existence of still other types of carriers, provided that we can understand why they have not been seen. We will now discuss evidence which supports the existence of a second type of heavy carrier, as yet undetected.

Zitter's low-field galvanomagnetic measurements[27] detect only two types of carriers, with $q_e=3$, $q_h=1$, and $N_e'=2.5\times10^{17}$ cm^{-3}. Such measurements cannot, however, furnish any information about carriers of mobility very much less than that of the light electrons and light holes in the field range $H\approx1$ G. As we have seen, some heavy carriers must be present to account for the greater part of the specific heat. Now Zitter sees equal numbers of light electrons and light holes (within 20%). Therefore, we may add heavy carriers of one sign to his model only if we also add an equal number of heavy carriers of opposite sign. Reconciliation of Zitter's results with ours thus requires abandoning a two- or three-carrier model in favor of a four-carrier model. From this point of view, the two experiments may be regarded as complementary. On the one hand, the galvanomagnetic measurements are quite insensitive to any carriers which carry less than a few percent of the current in the low-field range. Such carriers are likely to be heavy, with small Fermi energies, and hence to be precisely those carriers which make the greatest contribution to the specific heat. The Shubnikov-de Haas measurements, on the other hand, have revealed the existence of one such group of carriers, but in no way impose the condition that there be no other group of heavy carriers. Such a second group might not have been observed because the periods associated with its Fermi surface are too small.

In the event that there are four types of carriers, we must modify Eqs. (9) and (10). Equation (9) becomes, for example,

$$q_en_e'+q_En_E=q_hn_h+q_Hn_H. \tag{11}$$

[58] J. R. Sybert, C. G. Grenier, and J. M. Reynolds, Bull. Am. Phys. Soc. 7, 74 (1962).

Here the subscript H is reserved specifically for the heavy holes, and the subscript E refers to the heavy electrons.

If we assume, with Zitter, that $q_e=3$ and $q_h=1$, we find, as does Zitter, that $N_e'\approx N_h$. Hence, as we have remarked, $N_E\approx N_H$. However, q_E and q_H may not both be equal to unity, for this set of q's leads by a symmetry argument to a superposition of at least two of the bands H, h, and E.[59] We have eliminated this possibility in the discussion of the three-carrier models. It follows that $q_E+q_H\geqslant 3$. Since the Shubnikov-de Haas effect does not distinguish between electrons and holes, we will refer to the observed and the postulated heavy carriers with the subscripts 1 and 2. Calculation leads to the parameters for the four-carrier model which are given in Table V.

If we have seen the heavy-carrier Fermi surface for which $q_1\geqslant 2$, it follows that $q_2\geqslant 1$. For the sake of simplicity, we assume that the equality holds. Since $N_1\approx N_2$, we have $n_2/n_1=2$. As $P\propto A^{-1}$, Eq. (8) yields $P_2^*/P_1=(n_1/n_2)^{\frac{2}{3}}$, where P^* is an appropriate average Shubnikov-de Haas oscillation period. We may conclude that $P_2^*\approx 0.6P_1=0.4\times 10^{-5}$ G^{-1}. Such a value of P_2^* is almost certainly too small to have been seen in our experiment; note that we were unable to observe the electron period $P_1=0.5\times 10^{-5}$ G^{-1} in the binary directions.

V. SUMMARY AND CONCLUSIONS

By employing a sensitive differential technique, we have been able to observe directly a group of heavy carriers in bismuth, in addition to the light electrons and light holes previously observed. These heavy carriers make it possible to account for the large observed values of the carrier specific heat. We are able to derive the concentration of heavy carriers per ellipsoid n_H directly from the experimental data; we may derive n_e' and n_h from our data by adducing cyclotron resonance and de Haas-van Alphen results. Upon the assumption that there are no other carriers in bismuth, we may determine two possibilities for the ellipsoid multiplicities q and the total carrier concentrations N; adducing experimental values of the specific heat leads to values for the heavy carrier effective mass and Fermi energy.

Both of the three-carrier models thus obtained are irreconcilable with the values of q_e and q_h deduced by Zitter. We have, however, succeeded in bringing our results and Zitter's into agreement on the basis of a four-carrier model without doing violence to any of the published experimental results. The situation in bismuth is thus similar to that in antimony, in which there appear to be at least three, and very likely four, types of carriers.[60]

The observation of anomalies in the oscillations for magnetic field orientations near the binary axis indicates that there are likely to be fundamental differences between the theory of the de Haas-van Alphen effect and a detailed theory of the Shubnikov-de Haas effect.

ACKNOWLEDGMENTS

The author wishes to express his gratitude to his research sponsor, Professor A. W. Lawson, for continued interest and encouragement, and to Professor M. H. Cohen, Dr. M. G. Priestley, Dr. L. Falicov, and Professor H. Fritzsche for enlightening discussions on numerous aspects of the problem.

Note added in proof. We are grateful to R. N. Zitter for pointing out that his results (reference 27) strictly preclude a three-carrier model of the Fermi surface of bismuth, regardless of the values assumed for q_i.

[59] The only two points in the Brillouin zone (Fig. 1) which may be occupied by a Fermi surface for which $q=1$ are the center and the intersection of the trigonal axis with the zone face.

[60] C. A. Nanney (private communication).